HHS Public Access

Author manuscript

Nat Med. Author manuscript; available in PMC 2016 October 04.

Published in final edited form as:

Nat Med. 2016 May ; 22(5): 531–538. doi:10.1038/nm.4073.

Inflammatory signaling in human Tuberculosis granulomas is spatially organized

Mohlopheni J. Marakalala[*,1], **Ravikiran M. Raju**[*,1], **Kirti Sharma**[*,2], **Yanjia J. Zhang**[*,1], **Eliseo A. Eugenin**[3,10], **Brendan Prideaux**[3], **Isaac B. Daudelin**[3], **Pei-Yu Chen**[3], **Matthew G. Booty**[4,5], **Jin Hee Kim**[6], **Seok Yong Eum**[7], **Laura E. Via**[8,9], **Samuel M. Behar**[4], **Clifton E. Barry III**[8,9], **Matthias Mann**[2], **Véronique Dartois**[^,3,10], and **Eric J. Rubin**[^,1]

[1]Department of Immunology and Infectious Disease, Harvard T.H. Chan School of Public Health, Boston, MA, USA

[2]Department of Proteomics and Signal Transduction, Max Planck Institute of Biochemistry, Am Klopferspitz 18, Martinsried, Germany

[3]Public Health Research Institute, New Jersey Medical School, Newark, NJ, USA

[4]Department of Microbiology and Physiological Systems, University of Massachusetts Medical School, Worcester, MA, USA

[5]Program in Immunology, Division of Medical Sciences, Harvard Medical School, Boston, MA, USA

[6]National Masan TB Hospital, Changwon, Republic of Korea

[7]International Tuberculosis Research Center, Changwon, Republic of Korea

[8]Tuberculosis Research Section, Laboratory of Clinical Infectious Disease, National Institute of Allergy and Infectious Disease, National Institutes of Health, Bethesda, MD 20892 and Institute of Infectious Disease and Molecular Medicine

[9]Department of Clinical Laboratory Sciences, Faculty of Health Sciences, University of Cape Town, Rondebosch 7701, Republic of South Africa

[10]Department of Microbiology and Molecular Genetics, New Jersey Medical School, Rutgers The State University of New Jersey, Newark, NJ, USA

^to whom correspondence should be addressed: ; Email: erubin@hsph.harvard.edu and ; Email: dartoiva@njms.rutgers.edu

*these authors contributed equally; arranged alphabetically

Accession codes

The mass spectrometry proteomics data have been deposited to the ProteomeXchange Consortium (http://proteomecentral.proteomexchange.org) via the PRIDE partner repository with the dataset identifier PXD003646.

Contributions

M.J.M., R.M.R., K.S., Y.J.Z., E.A.E., B.P., M.M., V.D. and E.J.R. designed experiments. M.J.M., R.M.R., K.S., Y.J.Z., E.A.E., B.P., I.B.D., P.-Y.C. and L.E.V. performed experiments and analyzed data. M.J.M., K.S., Y.J.Z., E.A.E. and B.P. prepared the figures: M.G.B., J.H.K., S.Y.E., L.E.V., S.M.B. and C.E.B. contributed clinical samples and intellectual expertise. M.J.M., R.M.R., Y.J.Z., V.D. and E.J.R. wrote the manuscript: All authors read the manuscript and approved the submission.

Competing financial interests

There is NO competing interest

Abstract

Granulomas are the pathological hallmark of tuberculosis (TB). However, their function and mechanisms of formation remain poorly understood. To understand the role of granulomas in TB, we analyzed the proteomes of granulomas from subjects with tuberculosis in an unbiased fashion. Using laser capture microdissection, mass spectrometry and confocal microscopy, we generated detailed molecular maps of human granulomas. We found that the centers of granulomas possess a pro-inflammatory environment characterized by anti-microbial peptides, ROS and pro-inflammatory eicosanoids. Conversely, the tissue surrounding the caseum possesses a comparatively anti-inflammatory signature. These findings are consistent across a set of six subjects and in rabbits. While the balance between systemic pro- and anti-inflammatory signals is crucial to TB disease outcome, here we find that these signals are physically segregated within each granuloma. The protein and lipid snapshots of human and rabbit lesions analysed here suggest that the pathologic response to TB is shaped by the precise anatomical localization of these inflammatory pathways during the development of the granuloma.

Introduction

Tuberculosis (TB), caused by the bacterial pathogen *Mycobacterium tuberculosis* (MTB), remains a major global health problem responsible for 1.5 million deaths annually[1]. When the pathogen seeds the lung, both bacterial and host factors induce tissue remodeling, creating chronic inflammatory lesions known as granulomas[2,3].

Initially, granulomas are formed as aggregates of innate immune cells that are recruited to the site of infection. These include macrophages that later differentiate into specialized cell types, including multinucleated giant cells and epithelioid macrophages. Upon the development of adaptive immunity, granulomas acquire a more intact structure with the macrophage-rich center surrounded by T cells and B cells resulting in a lymphocytic cuff at the periphery of the structures [4–8]. With time, however, some granulomas can undergo complex remodeling characterized by the accumulation of necrotic material that leads to the formation of caseum at the center. The caseum may undergo liquefaction resulting in cavitation – the destructive fusion of a liquefying granuloma with an adjacent airway –, which facilitates bacterial dissemination[9–12]. It is still poorly understood whether tuberculous granulomas represent a host strategy for bacterial control or dynamic immune structures that facilitate bacterial transmission, or both[7,8,13,14].

Although the histology of this progression of granulomas has been well characterized, the molecular and inflammatory signatures that accompany granuloma progression have been poorly described. The granuloma is a functional paradox: it reflects an impressive deployment of immune cells that serves to contain the invading pathogen but it often fails to eradicate the persistent organisms. If containment fails completely, it serves as a shell within which bacilli find nutrients and protection to replicate without restriction[15,16]. Recent data in human disease and primate models show that infected individuals have a heterogeneous mixture of granulomas that may vary greatly in the degree of immune activation and presumed bacterial control[17]. Thus, it is increasingly recognized that the fate of a few granulomas contributes to the majority of clinical morbidity[10,18,19]. These data suggest that

important disease-driving processes are compartmentalized within individual granulomas and that variations within and among these structures are associated with disease control and progression.

To understand granuloma formation and progression in higher resolution and in an unbiased fashion, we employed approaches to assess the distribution of molecules in different types of granulomas as well as in different cell types. By combining laser micro-dissection, mass spectrometry and confocal microscopy, we have analyzed the abundance of proteins and lipids during the different stages of granuloma with exquisite anatomical localization giving us a molecular map of the human granuloma. We found that pro-inflammatory enzymes that generate lipid-based inflammatory factors, such as eicosanoids, were enriched in both the necrotic centers as well as the cells that immediately border the caseum. Animal models have highlighted that both insufficient inflammation and excessive inflammation can each promote progression of mycobacterial disease[20–24]. In humans, we find that both types of signaling occur simultaneously but are in anatomic distinct compartments within the granuloma. Our results suggest unique molecular signatures between different kinds of compartments within granulomas. We propose that this local balance between anti- and pro-inflammatory lipid mediators affects the capacity of the host to resolve or isolate the pathogen during infection in the lung.

Results

The proteomic architecture of human TB granulomas

We sought to identify candidate proteins that were differentially distributed in anatomically distinct compartments in the tuberculous lung. To do this, we isolated human granulomas from HIV- subjects undergoing pneumonectomy for multi-drug resistant TB (Supplemental Table 1a). Using lung samples from several individuals as well as granulomas from the same lung in different stages of differentiation, we classified these lesions according to histology as solid granulomas that lacked necrosis, caseous granulomas, and cavitary granulomas (Figure 1a **and** Supplemental Table 1b). We selected one representative lesion of each type for whole proteome analysis. For each granuloma, we used laser-guided microdissection to separate histologically distinct areas, which allowed us to define the proteome of five separate granuloma regions. These included the interior of a solid granuloma, the cellular borders of the caseous and cavitary granulomas, as well as the necrotic caseum of the caseous and cavitary granulomas (Supplemental Figure 1a).

We analyzed the five proteomes using quantitative mass spectrometry and label-free protein quantification to compare the relative abundance of proteins (Figure 1b). Combined analysis of all microdissected granuloma regions identified more than 30,000 sequence unique tryptic peptides, which assembled into 4,406 proteins (Supplemental Table 2). This corresponds to an average of 3,774 different proteins in each of these samples, of which more than 3,500 proteins were identified in at least four of the five samples (Figure 1c, Supplemental Figure 1b, Supplemental Figure 2a and 2b). We used these data to create a spatially resolved map of protein expression in human granulomas.

Higher proteomic diversity within than between granulomas

We hypothesized that, as granulomas progress through stages, we would find marked proteomic similarities between different types of granulomas. Surprisingly, our most striking finding was that there was far more variation within granulomas than between granuloma subtypes. Using unsupervised hierarchical clustering, we found that the cellular regions of granulomas, regardless of the type of lesion from which they were excised, clustered together, as did the caseous regions (Figure 2a and Supplemental Figure 2a). Principal component analysis revealed a similar grouping (Figure 2b).

Inflammatory signaling distinguishes caseum from cellular rim

To determine the biological processes that separate the caseum from the cellular periphery, we searched for Gene Ontology (GO) terms and Kyoto Encyclopedia of Genes and Genomes (KEGG) pathways enriched in the necrotic caseum. The functional protein groups most associated with the caseum included inflammatory and anti-microbial processes (Figure 2c). Known anti-mycobacterial effectors such as the anti-microbial peptide cathelicidin, activators of reactive oxygen species, and anti-microbial effectors downstream of TNF and IFN signaling localized to the caseum (Figure 2d Supplemental Figure 2c, Supplemental Table 3). Notably, proteins involved in the production of pro-inflammatory eicosanoids were also more abundant in the caseum. (Figure 2e). The cellular periphery of the granuloma was enriched for processes involved in protein synthesis, including ribosomal and endoplasmic reticulum proteins (Supplemental Table 3). This is consistent with the histological appearance of the periphery, which contains intact cells that we expected to be highly metabolically active. Collectively, these findings are consistent with a pro-inflammatory signature within the caseum. While it contains little synthetic activity, the caseum is filled with anti-microbial effectors that suggest remnants of a robust immune response against the pathogen.

Arachidonic acid is released throughout the granuloma

Our proteomics data suggests a role for the proteins that metabolize arachidonic acid, including ALOX5, ALOX5AP and LTA4H (Figure 2e). These proteins were more enriched in the caseum suggesting that eicosanoids, products of arachidonic acid and key mediators of inflammation during TB infection, could play an important role (Supplemental Figure 3a). Within the proteome we found an abundance of phospholipase A2 activating protein, which activates enzymes involved in synthesizing the eicosanoid precursor arachidonic acid (AA) (Supplemental Figure 3b). We were unable to detect all of the phospholipases involved in eicosanoid production using MS-MS. Thus, we used immunohistochemistry and confocal microscopy to localize multiple phospholipases involved in the production of AA-containing lysophospholipids. We found that most were diffusely expressed throughout the granulomas (Supplemental Figure 3c).

Though the presence of detectable biosynthetic enzymes suggests that their end products likely accumulate, the abundance of enzymes and their products might not correlate since enzyme activity is regulated in multiple ways. To test this, we directly measured the abundance of AA using MALDI-MS imaging (Figure 3a). We imaged both AA and AA precursors in human cellular, caseous and cavitary granulomas (Supplemental Table 1c), and

found their abundance pattern to mirror the expression of the proteins that metabolize AA as determined by proteomics analysis. While little AA was detected in normal lung tissue, AA synthesis occurs throughout the granuloma, with enrichment at the borders of the caseum (Figure 3b). Notably, MALDI-MS imaging of tissues from rabbit solid and caseous tissues revealed similar patterns of AA distributions as those in human granulomas (Figure 3c).

Caseous foci contain high amounts of inflammatory eicosanoids

AA is the key synthetic precursor for eicosanoids but much previous work suggests that AA can enter either pro-inflammatory or anti-inflammatory pathways [25,26](Figure 4a). Since our proteomic analysis demonstrated a predominant inflammatory signature at the necrotic center of granulomas, we reasoned that while AA was diffusely present, it would preferentially be utilized for generation of pro-inflammatory eicosanoids near the center of granulomas. Leukotriene-A4 Hydrolase (LTA4H) synthesizes leukotriene B4 (LTB4), a pro-inflammatory eicosanoid that has been associated with production of TNF-α. TNF-α is a key component of early host control of bacterial growth[27–29], but its excess has also been implicated in tuberculosis immunopathogenesis in zebrafish and humans[21,30]. By MS proteomics, we found that LTA4H was highly abundant in the caseum, along with enzymes necessary for synthesizing other leukotriene precursors (Figure 2E). By immunohistochemistry, we also found LTA4H within caseum and the caseous margins of cavitary lesions (Figure 4b and Supplemental Figure 4). Notably, there was little staining in the solid granuloma, consistent with low representation of a pro-inflammatory proteome signature in this granuloma (Figure 4b, 4c).

LTA4H was also expressed in the cellular borders of the caseous and cavitary granulomas, though in a very specific pattern. We found that LTA4H was most abundant in cells immediately adjacent to the caseum, and that expression decreased as a function of distance from the necrotic center (Figure 4b, 4d). This region is largely composed of macrophages. Unnecessary. Please delete if you have not directly shown this. We identified the various morphologic subtypes to determine which cells were responsible for LTA4H expression at the cellular border of the caseum. We found that giant cells expressed high levels of the enzyme (Figure 4e). In the solid granuloma, which contained very little LTA4H overall, the only expression was found in a small cluster of giant cells at the periphery of the granuloma (Figure 4b, 4e). Using a macrophage specific surface marker, we also found finger-like projections of macrophages into the necrotic caseum. Interestingly, these macrophage projections also highly co-localized with LTA4H (Figure 4e). This suggests that morphologically distinct macrophage populations near the necrotic border may control the gradient of LTA4H expression and help generate a highly inflammatory milieu contained at the center of the granuloma. (Refer to Methods (Immunohistochemistry section), where we explain how different regions were delineated).

In zebrafish TB models, excess LTA4H has been shown to promote macrophage necrosis through the induction of TNF-α production[21]. We reasoned that this pro-inflammatory cytokine would be more abundant and, likely, co-localize with LTA4H in the regions where granulomas are necrotizing. Indeed, our immunohistochemistry showed that TNF-α was relatively less abundant in solid granulomas (Figure 5a), but more abundant in the necrotic

margins of caseous and cavitary granulomas (Figure 5b, 5c, and Supplemental Figure 5a). Interestingly, TNF-α staining revealed distributions similar to LTA4H, with a co-localization of ~85.3%. We also found that the co-localization of LTA4H and TNF-α was recapitulated in rabbit solid and caseous lesions (Figure 5d, Supplemental Figure 5b). These results suggest that the spatial LTA4H-mediated pro-inflammatory responses are associated with TNF-α production.

Cellular rims and solid lesions exhibit an anti-inflammatory signature

In contrast to the centers of necrotic granulomas, cells found at the periphery of granulomas contained a more anti-inflammatory proteomic signature. Specifically, anti-inflammatory regulators and reducing agents were enriched in the granuloma periphery (Figure 2d). In the eicosanoid pathway, prostanoid synthesis moderates inflammation in TB lesions [21,22,24] (Figure 6a). We observed that enzymes responsible for prostanoid synthesis, namely cyclo-oxygenase 1 and 2 (COX1/2), were enriched in the solid granuloma, consistent with the overall less inflammatory signature of that granuloma (Figure 6b). The distribution of proteins was similar to the distribution of products, as measurement of prostanoid concentrations by HPLC coupled to tandem mass spectrometry showed that they, too, were more abundant in cellular layers (Figure 6c, Supplemental Figure 6a).

In cavitary and caseous granulomas we found that both COX1 and COX2 were diffusely expressed in the cellular layers but largely absent in the necrotic caseum (Figure 6d, 6e, Supplemental Figure 6b). This contrasts with the pattern of LTA4H abundance. Additionally, while LTA4H was specifically expressed by macrophage subsets, we found COX1/2 expression in both macrophages and fibroblasts (Figure 6f). In rabbit tissues, we found that COX1/2 was more abundant in cellular regions and less in the necrotic caseum, recapitulating the observations in human lesions (Figure 6g, 6h and Supplemental Figure 6d), in contrast to TNF-α and LTA4H (Supplemental Figure 6c). Thus, the relative abundance of various eicosanoids (leukotrienes) suggests a highly pro-inflammatory center of the granuloma surrounded by a cuff of molecules that moderate inflammation, including some prostanoids of the COX1/2 pathways.

Discussion

The host's ability to effectively respond to infection by MTB is perhaps the most crucial determinant of disease outcome. Numerous investigations have highlighted the various axes, both genetic and temporal, that tip the scale in favor of either host or pathogen[21]. Genetically, mutations in the leukotriene A4 hydrolase gene that results in reduced levels of the pro-inflammatory eicosanoid LTB4 led to increased mortality in zebrafish[21,31]. Temporally, TNF dually mediates resistance and susceptibility to mycobacteria by promoting the production of reactive oxygen species (ROS) by infected macrophages in granulomas. While ROS have an antimicrobial effect, they ultimately promote necrosis of immune cells and growth of bacteria[30].

Here, we find that the spatial organization of pro- and anti-inflammatory mediators defines a third critical axis. Critical effector molecules that serve as mediators of inflammation are specifically localized at sites of MTB infection. The abundance of LTA4H, alongside the

pro-inflammatory cytokine TNF-α, were highest in the necrotic centers of granulomas, as were ROS mediators and antimicrobial effectors such as cathelicidin. Conversely, prostanoids and their biosynthetic machinery, the cyclooxygenases [25,26,20,22], were most concentrated around areas of necrosis. These data need to be interpreted in a clinical context. All granulomas were obtained from individuals that underwent pneumonectomy because of severe TB, and hence have extensive tissue damage. Also, neither the age of each lesion nor its ultimate fate is known. Despite these limitations, the spatial distribution and organization of the molecules we identified suggest that the inflammatory and antimicrobial effects known to be required to combat infection, but are potentially destructive to host tissues, are contained, and possibly restrained, by a ring of anti-inflammatory activity. We hypothesize that this anatomical organization promotes antibacterial activity while limiting tissue destruction.

One limitation of our study is the small number of subjects and individual lesions we could examine. Moreover, all of these patients had pulmonary resections for TB infections that could not be controlled with medical management alone and, therefore, likely represent the most severe end of the spectrum of pulmonary TB. However, our findings are likely to be broadly representative. We find that even the evolutionarily distant rabbit model reveals a similar granuloma microarchitecture.

A number of computational models of TB granulomas have explored the dynamics of pro- and anti-inflammatory cytokines across spatial and temporal axes[32–34]. At a cellular scale, TNF-α is thought to play a role in the activation of resting macrophages and inhibition of bacterial dissemination. However, hyper-inflammation associated with this cytokine may lead to cell death and lung tissue damage[21,32]. IL-10 might play a role in controlling the trade-off between the anti-microbial activity and host-derived tissue caseation[33,34]. Other studies, involving animal models and human blood signatures, have demonstrated that a cross-regulatory network of eicosanoids and cytokines may operate during infection to provide optimal protection [20,35]. In humans, our data suggest that pathways that mediate the spatial balance of inflammation play a similar role in limiting the degree of immunopathology. We suggest that a causal link between the outcome of infection and the signaling molecules mapped in this study is likely, and that modeling must take the spatial organization of host responses into account to guide the development of host-directed therapies that maintain effective pro- and anti-inflammatory levels.

Obtaining such a window into the local interplay of mediators during infection has been limited so far by methodological challenges. Traditionally, the structure of the human granuloma has been interrogated using cell-based histological markers and immunohistochemistry that identify a narrow array of cellular proteins[4,5]. Newer, unbiased methods, such as quantitative mass spectrometry to identify and image the distribution of lipid and proteins present within a granuloma, can both increase the resolution and the depth of histological analysis [36,37,38]. These provide information about cell types that are present and also about their metabolic states. Here, we identified over 3000 proteins; the number of lipid species that can be identified is limited only by their abundance and the availability of standards. The organization of inflammatory mediators shows how unbiased molecular tools can uncover new biological principles.

Taken together, our human and rabbit findings suggest that the ability of the host to contain MTB and restrict host damage is a localized phenomenon at the level of individual granulomas. Certainly, marked differences in bacterial burden and immune activation exist between granulomas even within one host[19,39]. TB is not a monomorphic disease; instead, it proceeds differently in each individual lesion. Host-directed therapies such as ALOX-5 inhibitors, LTB4 receptor antagonists and some corticosteroids, that push the pro- and anti-inflammatory balance in one direction or another, provide an attractive model for therapies that limit host damage and assist in controlling infection[20–24,40]. While our results require confirmation in larger sample sets, the data suggest that the real balance occurs locally and that systemic interventions could be quite complex.

Supplementary Material

Refer to Web version on PubMed Central for supplementary material.

Acknowledgments

We would like to thank the patients and staff of National Masan TB Hospital, South Korea, as well as the technical staff from the International Tuberculosis Research Center, Masan, South Korea, for their participation in our studies. We also acknowledge Amanda Martinot for generating some of the H&E images and for useful advices on pathology studies; and members of the Rubin and Fortune labs for useful discussions. This work was supported by a Visiting Science Award from HHMI/K-RITH (EJR), US National Institutes of Health (NIH) grant 1S10OD018072-01A1 (shared instrumentation grant for the MALDI orbitrap) and US Bill and Melinda Gates Foundation TB Drug Accelerator grant #OPP 1066499 (VD), NIH grant R01AI098637 (SMB), Division of Intramural Research, National Institute of Allergy and Infectious Disease, NIH and the Korean Centers of Disease Control, Ministry of Health, Welfare and Family Affairs (CEB), and National Institute of Mental Health grant, MH096625, and US Public Health Research Institute (New Jersey Medical School) central grant (EAE). We would like to acknowledge the PRIDE Team for upload of proteomics raw data.

References

1. World Health Organization. Tuberculosis: Fact Sheet No: 104. 2015.
2. Taylor JL, et al. Role for matrix metalloproteinase 9 in granuloma formation during pulmonary Mycobacterium tuberculosis infection. Infect Immun. 2006; 74:6135–6144. [PubMed: 16982845]
3. Volkman HE, et al. Tuberculous granuloma induction via interaction of a bacterial secreted protein with host epithelium. Science. 2010; 327:466–469. [PubMed: 20007864]
4. Ulrichs T, et al. Human tuberculous granulomas induce peripheral lymphoid follicle-like structures to orchestrate local host defence in the lung. J Pathol. 2004; 204:217–228. [PubMed: 15376257]
5. Ehlers S, Schaible UE. The granuloma in tuberculosis: dynamics of a host-pathogen collusion. Front Immunol. 2012; 3:411. [PubMed: 23308075]
6. Evelyn Guirado LSS. Modeling the Mycobacterium tuberculosis Granuloma – the Critical Battlefield in Host Immunity and Disease. Front Immunol. 2013; 4:98. [PubMed: 23626591]
7. Mattila JT, et al. Microenvironments in tuberculous granulomas are delineated by distinct populations of macrophage subsets and expression of nitric oxide synthase and arginase isoforms. J Immunol. 2013; 191:773–784. [PubMed: 23749634]
8. Ramakrishnan L. Revisiting the role of the granuloma in tuberculosis. Nat Rev Immunol. 2012; 12:352–366. [PubMed: 22517424]
9. Cardona PJ. A spotlight on liquefaction: evidence from clinical settings and experimental models in tuberculosis. Clin Dev Immunol. 2011; 2011:868246–9. [PubMed: 21437230]
10. Kim MJ, et al. Caseation of human tuberculosis granulomas correlates with elevated host lipid metabolism. EMBO Mol Med. 2010; 2:258–274. [PubMed: 20597103]
11. Kaplan G, et al. Mycobacterium tuberculosis growth at the cavity surface: a microenvironment with failed immunity. Infect Immun. 2003; 71:7099–7108. [PubMed: 14638800]

12. Subbian S, et al. Lesion-Specific Immune Response in Granulomas of Patients with Pulmonary Tuberculosis: A Pilot Study. PLoS ONE. 2015; 10:e0132249. [PubMed: 26133981]
13. Bold TD, Ernst JD. Who benefits from granulomas, mycobacteria or host? Cell. 2009; 136:17–19. [PubMed: 19135882]
14. Davis JM, Ramakrishnan L. The role of the granuloma in expansion and dissemination of early tuberculous infection. Cell. 2009; 136:37–49. [PubMed: 19135887]
15. Peyron P, et al. Foamy macrophages from tuberculous patients' granulomas constitute a nutrient-rich reservoir for M. tuberculosis persistence. plos pathogens. 2008; 4:e1000204. [PubMed: 19002241]
16. Saunders BM, Cooper AM. Restraining mycobacteria: Role of granulomas in mycobacterial infections. Immunology and Cell Biology. 2000; 78:334–341. [PubMed: 10947857]
17. Via LE, et al. Infection dynamics and response to chemotherapy in a rabbit model of tuberculosis using [^{18}F]2-fluoro-deoxy-D-glucose positron emission tomography and computed tomography. Antimicrob Agents Chemother. 2012; 56:4391–4402. [PubMed: 22687508]
18. Lin PL, et al. Sterilization of granulomas is common in active and latent tuberculosis despite within-host variability in bacterial killing. Nat Med. 2014; 20:75–79. [PubMed: 24336248]
19. Gideon HP, et al. Variability in tuberculosis granuloma T cell responses exists, but a balance of pro- and anti-inflammatory cytokines is associated with sterilization. plos pathogens. 2015; 11:e1004603. [PubMed: 25611466]
20. Mayer-Barber KD, et al. Host-directed therapy of tuberculosis based on interleukin-1 and type I interferon crosstalk. Nature. 2014; 511:99–103. [PubMed: 24990750]
21. Tobin DM, et al. Host Genotype-Specific Therapies Can Optimize the Inflammatory Response to Mycobacterial Infections. Cell. 2012; 148:434–446. [PubMed: 22304914]
22. Chen M, et al. Lipid mediators in innate immunity against tuberculosis: opposing roles of PGE2 and LXA4 in the induction of macrophage death. J Exp Med. 2008; 205:2791–2801. [PubMed: 18955568]
23. Divangahi M, et al. Mycobacterium tuberculosis evades macrophage defenses by inhibiting plasma membrane repair. Nature Immunology. 2009; 10:899–906. [PubMed: 19561612]
24. Divangahi M, Desjardins D, Nunes-Alves C, Remold HG, Behar SM. Eicosanoid pathways regulate adaptive immunity to Mycobacterium tuberculosis. Nature Immunology. 2010; 11:751–758. [PubMed: 20622882]
25. Serhan CN. Pro-resolving lipid mediators are leads for resolution physiology. Nature. 2014; 510:92–101. [PubMed: 24899309]
26. Serhan CN, Chiang N, Van Dyke TE. Resolving inflammation: dual anti-inflammatory and pro-resolution lipid mediators. Nat Rev Immunol. 2008; 8:349–361. [PubMed: 18437155]
27. Clay H, Volkman HE, Ramakrishnan L. Tumor necrosis factor signaling mediates resistance to mycobacteria by inhibiting bacterial growth and macrophage death. Immunity. 2008; 29:283–294. [PubMed: 18691913]
28. Flynn JL, et al. Tumor necrosis factor-alpha is required in the protective immune response against Mycobacterium tuberculosis in mice. Immunity. 1995; 2:561–572. [PubMed: 7540941]
29. Dambuza I, et al. Reactivation of M. tuberculosis infection in trans-membrane tumour necrosis factor mice. PLoS ONE. 2011; 6:e25121. [PubMed: 22132068]
30. Roca FJ, Ramakrishnan L. TNF dually mediates resistance and susceptibility to mycobacteria via mitochondrial reactive oxygen species. Cell. 2013; 153:521–534. [PubMed: 23582643]
31. Tobin DM, et al. The lta4h locus modulates susceptibility to mycobacterial infection in zebrafish and humans. Cell. 2010; 140:717–730. [PubMed: 20211140]
32. Fallahi-Sichani M, El-Kebir M, Marino S, Kirschner DE, Linderman JJ. Multiscale computational modeling reveals a critical role for TNF-α receptor 1 dynamics in tuberculosis granuloma formation. J Immunol. 2011; 186:3472–3483. [PubMed: 21321109]
33. Cilfone NA, et al. Computational modeling predicts IL-10 control of lesion sterilization by balancing early host immunity-mediated antimicrobial responses with caseation during mycobacterium tuberculosis infection. J Immunol. 2015; 194:664–677. [PubMed: 25512604]

34. Cilfone NA, Perry CR, Kirschner DE, Linderman JJ. Multi-scale modeling predicts a balance of tumor necrosis factor-α and interleukin-10 controls the granuloma environment during Mycobacterium tuberculosis infection. PLoS ONE. 2013; 8:e68680. [PubMed: 23869227]

35. McNab F, Mayer-Barber K, Sher A, Wack A, O'Garra A. Type I interferons in infectious disease. Nat Rev Immunol. 2015; 15:87–103. [PubMed: 25614319]

36. Prideaux B, et al. The association between sterilizing activity and drug distribution into tuberculosis lesions. Nat Med. 2015; 21:1223–1227. [PubMed: 26343800]

37. Cox J, et al. Accurate proteome-wide label-free quantification by delayed normalization and maximal peptide ratio extraction, termed MaxLFQ. Mol Cell Proteomics. 2014; 13:2513–2526. [PubMed: 24942700]

38. Prideaux B, et al. High-sensitivity MALDI-MRM-MS imaging of moxifloxacin distribution in tuberculosis-infected rabbit lungs and granulomatous lesions. Anal Chem. 2011; 83:2112–2118. [PubMed: 21332183]

39. Via LE, et al. A Sterilizing Tuberculosis Treatment Regimen Is Associated with Faster Clearance of Bacteria in Cavitary Lesions in Marmosets. Antimicrob Agents Chemother. 2015; 59:4181–4189. [PubMed: 25941223]

40. Tobin DM, Ramakrishnan L. TB: the Yin and Yang of lipid mediators. Curr Opin Pharmacol. 2013; 13:641–645. [PubMed: 23849093]

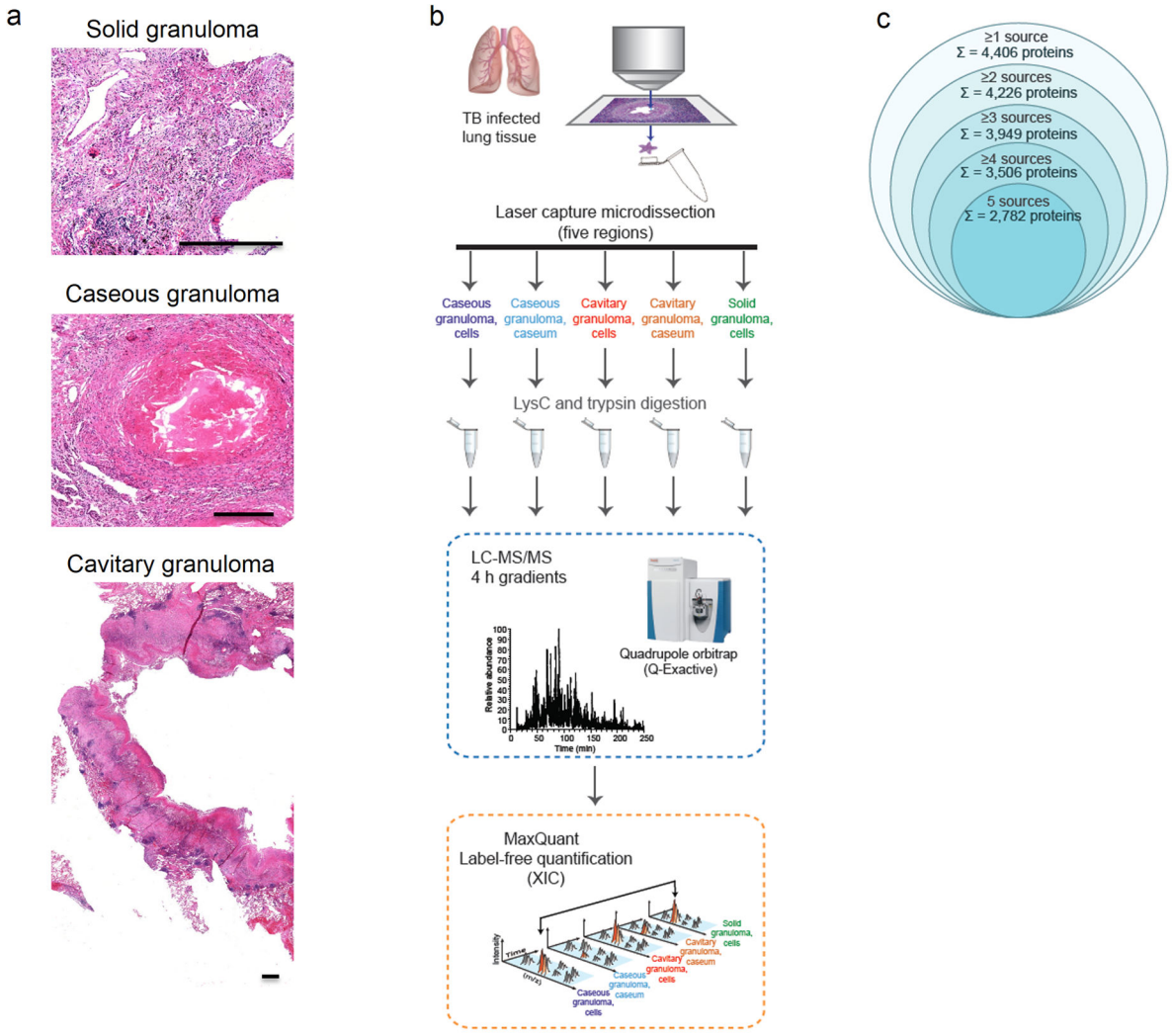

Figure 1. High resolution mass-spectrometry profiling of granuloma composition

(**a**) The three types of granulomas sampled in the study: solid, caseous and cavitary granulomas, scale bar = 1 mm. (**b**) Experimental workflow: laser capture micro-dissection was used to dissect, process and analyze multiple samples (n = 50 to 100, depending on the lesion compartment) in the caseous and cellular regions of each granuloma type. Dissected samples from each of the 5 regions were pooled and engaged in proteome-wide LC/MS-MS analysis. (**c**) A total of 4,406 proteins were identified across all granulomas and an average of ~95% protein identifications were shared between at least two proteomes. Five regions were sampled in three granuloma types from three different subjects. The proteomics data have been deposited to the ProteomeXchange Consortium (http://proteomecentral.proteomexchange.org) via the PRIDE partner repository with the dataset identifier PXD003646

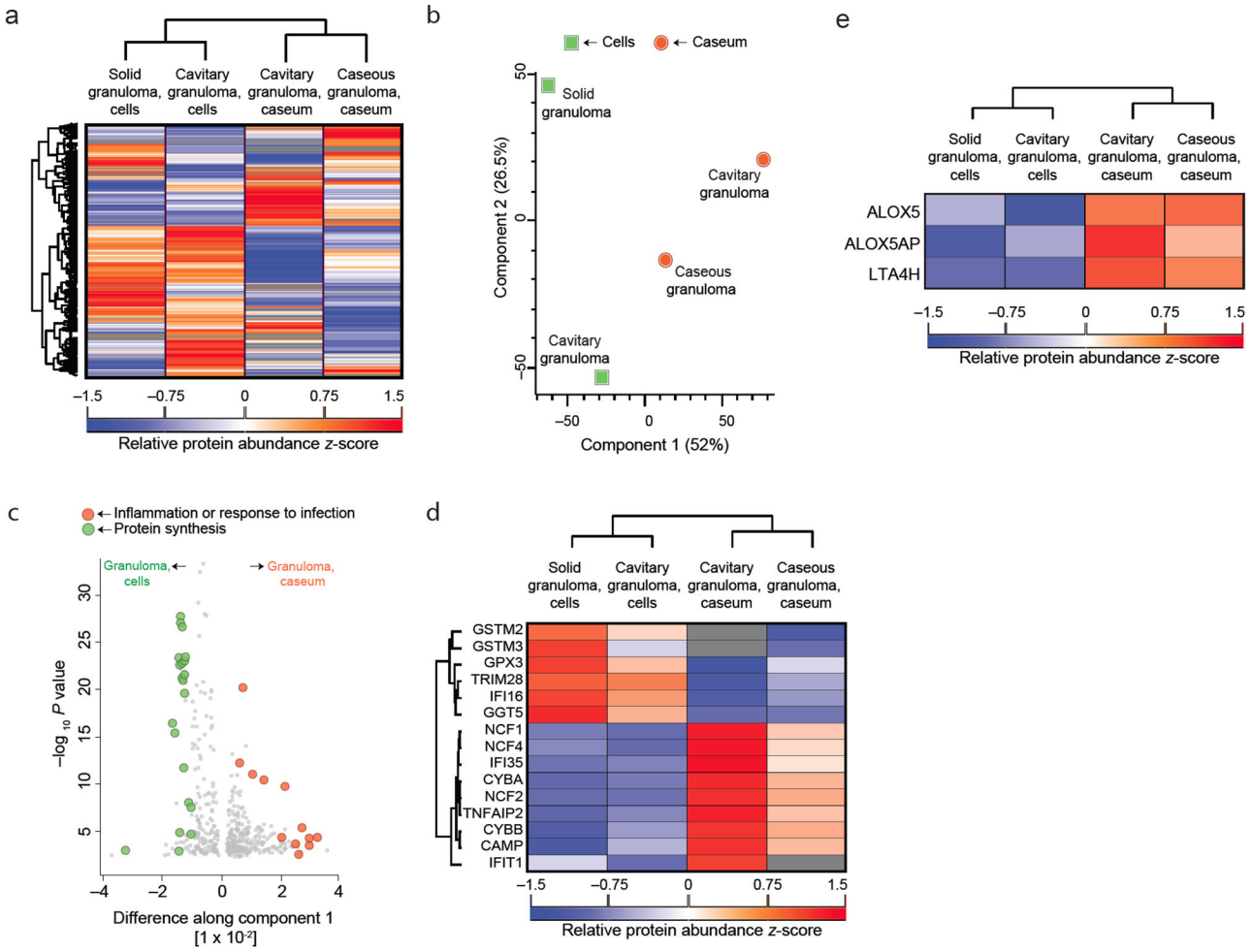

Figure 2. Quantitative proteome analysis reveals spatially distinct protein signatures in granuloma

(**a**) Hierarchical clustering analysis of 2,529 LFQ-protein intensities ($\log_2$) that were quantified in at least two of the five granuloma proteomes and showed at least a 1.5-fold difference in their abundance between at least two granuloma regions. Heatmap of z score- and $\log_2$-transformed LFQ protein intensities where proteins and granuloma regions were grouped using unsupervised hierarchical clustering. (**b**) Principal component analysis (PCA) separates necrotic caseum (orange circles) from cellular components (green squares) of granuloma. The first two components, which account for 52% and 26.5% of data variability from all granuloma regions, are shown. (**c**) Annotation terms (KEGG, GO, CORUM) of proteins significantly different along component 1 that separates necrotic caseum from cellular components. The scatter plot depicts the difference score of these terms versus the $-\log_{10}$-transformed *P* value. Annotation terms most associated with the necrotic caseum (orange circles) and cellular components (green circles) of granuloma are color coded. (**d**) Unsupervised hierarchical clustering based heat map of z score- and $\log_2$- transformed LFQ protein intensities for the indicated example pro-inflammatory proteins (labelled in orange font) and anti-inflammatory proteins (labelled in green). (**e**) Proteomic profiling of the leukotriene and lipoxin synthetic pathway. For statistical analyses, we tested and computed

the difference between medians of the two following groups: proteins corresponding to an annotation category versus all proteins in the dataset. We did this for every annotation term using two-sided Wilcoxon-Mann-Whitney test where the multiple hypothesis testing is adjusted by applying a Benjamini-Hochberg FDR threshold of 0.05.

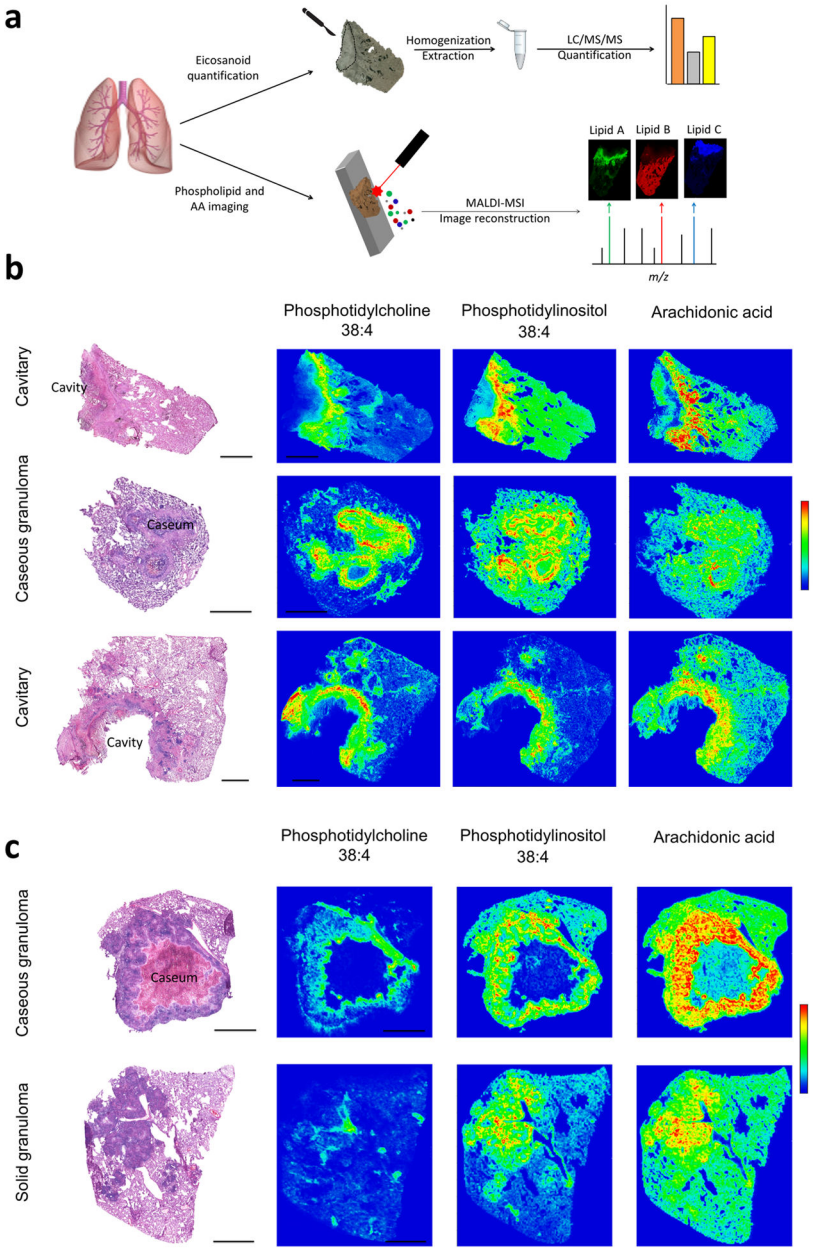

Figure 3. The eicosanoid precursor arachidonic acid (AA) is abundant and synthesized diffusely within all granulomas

(**a**) Workfhow of MALDI MS imaging and quantitation by LC/MS of membrane phospholipids and AA in dissected lesions. (**b**) MALDI MS imaging of AA-containing lipids and AA in human tissues. Three cavities and three caseous granulomas from six different subjects were imaged, and one representative lesion of each type is shown. (**c**) MALDI MS imaging of AA-containing lipids in rabbit tissues. Two solid and two caseous granulomas from four rabbits were imaged, and one representative lesion of each type is shown. Scale bar = 5 mm. Color bars show the image intensity ranging from blue (lowest) to red (highest).

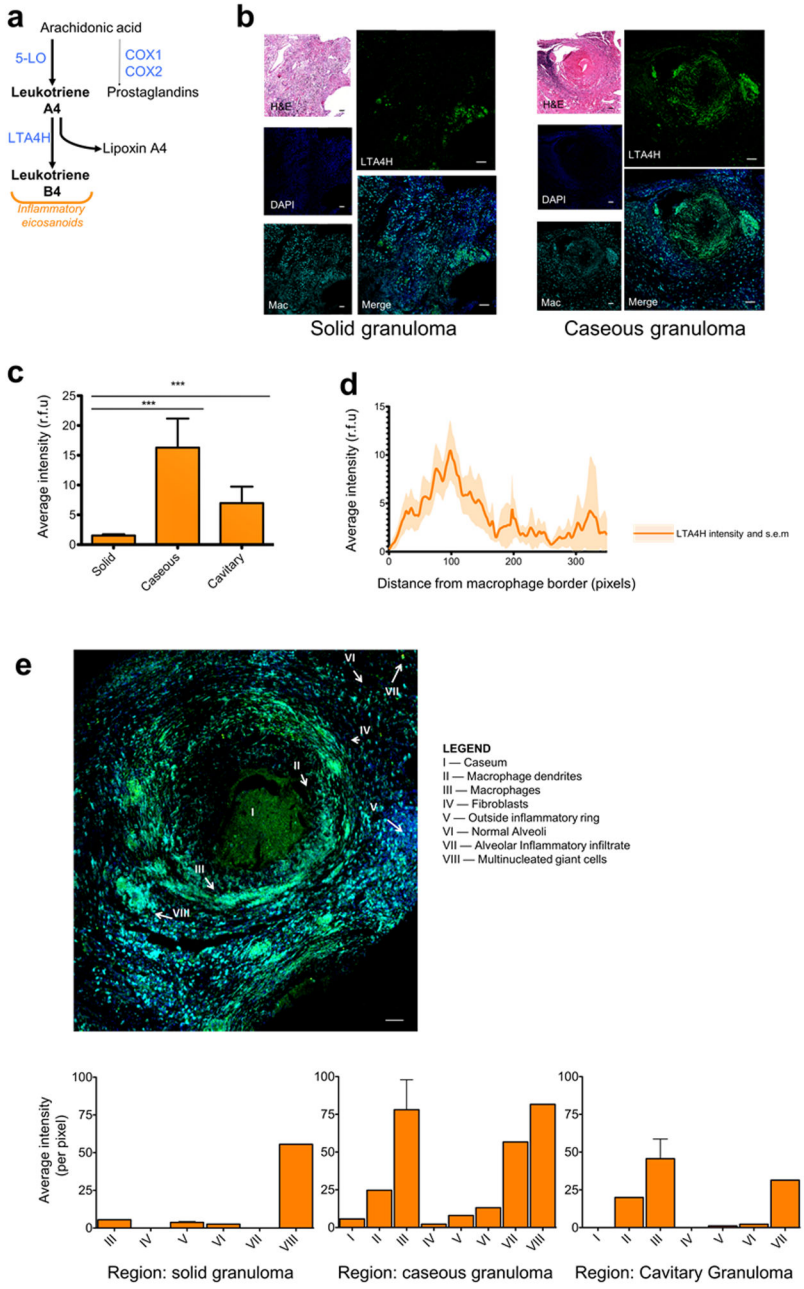

Figure 4. Leukotriene biosynthesis is enriched at in the caseum and the cellular layer directly adjacent to the caseum

(**a**) AA is the precursor for pro-inflammatory leukotrienes (left) or less inflammatory prostanoids (right). (**b**) H&E (upper left) and IHC staining of LTA4H (green), nuclei using DAPI (blue), and macrophages using IBA1 (cyan). (**c**) Average quantitation of LTA4H fluorescence in granulomas (n = 5). (**d**) Quantitation of LTA4H fluorescence as a function of distance from the macrophage border. (**e**) Relative intensity of LTA4H fluorescence in cellular subtypes within a typical caseous granuloma. Refer to Methods (Immunohistochemistry section) for explanations on how regions were delineated. All scale bars represent 350 um. For quantification of fluorescence average intensities in IHC images

(n = 22), a student's t-test was performed for single comparisons. For multiple comparisons, mean differences were tested by non-parametric Kruskal-Wallis analysis and adjusted by use of the Bonferoni-Dunn correction. *P* values of <0.05 were considered significant.

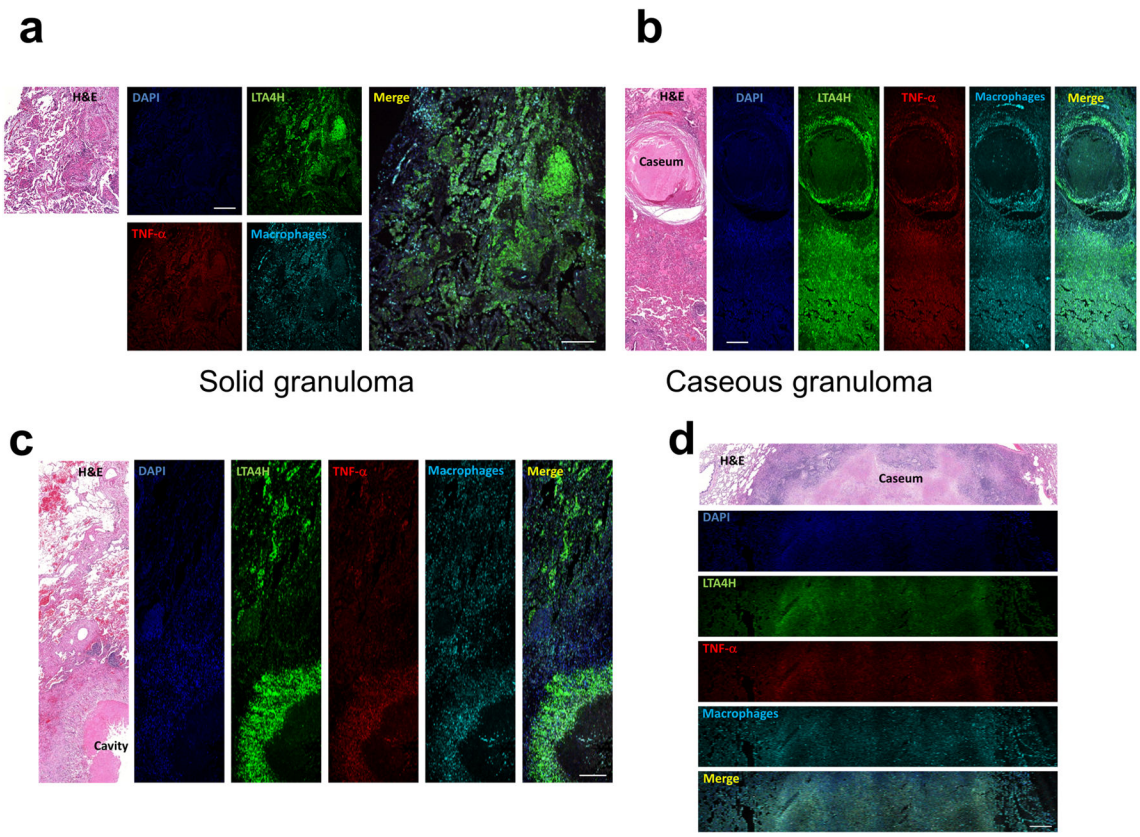

Figure 5. TNF-α and LTA4H are more abundant in the caseum and its margins

(**a**) IHC staining for TNF-α (red), LTA4H (green), nuclei using DAPI (blue), and macrophages using IBA1 (cyan) in a solid granuloma (n = 1). (**b**) IHC staining of one representative caseous granuloma (n=4). (**c**) IHC staining of one representative cavitary granuloma (n= 3). (**d**) IHC staining for TNF-α (red), LTA4H (green), nuclei using DAPI (blue), and macrophages using IBA1 (cyan) of a representative rabbit caseous granuloma (n = 2). All scale bars represent 350 um.

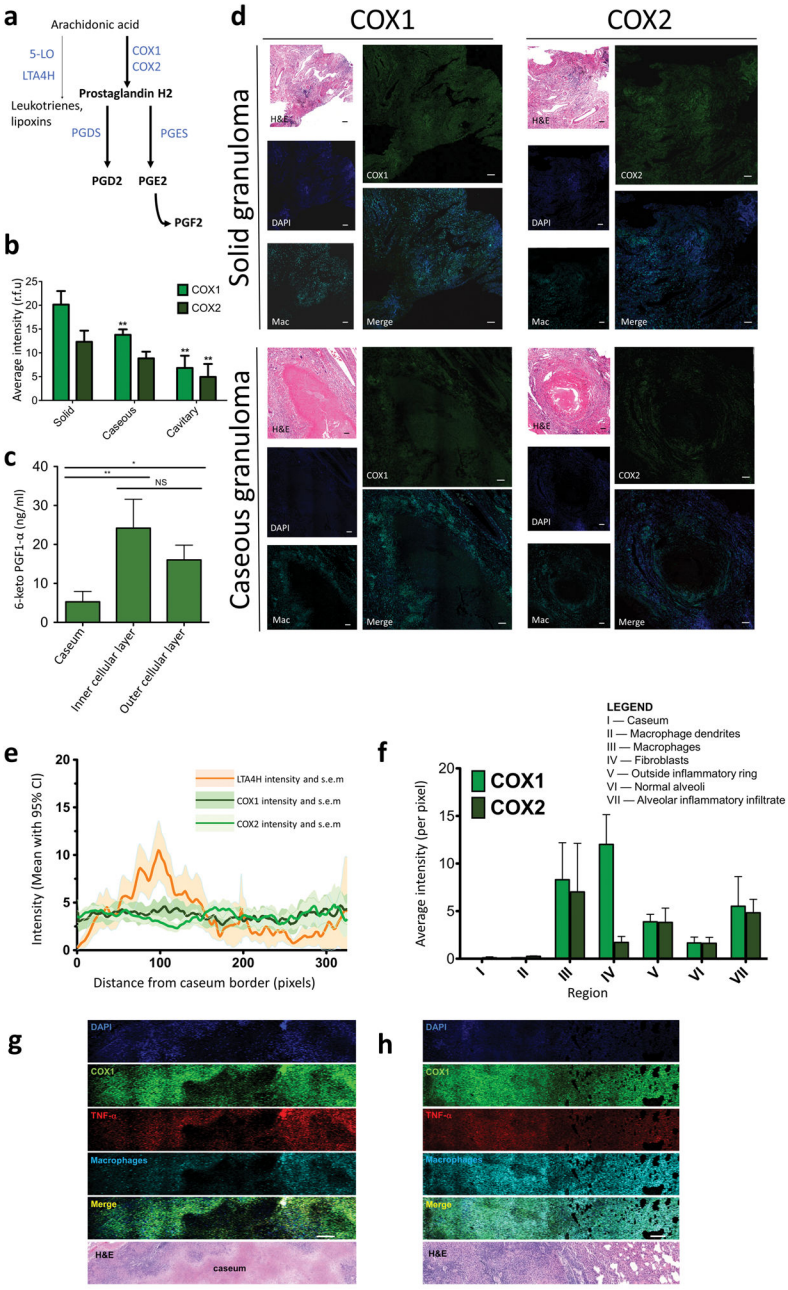

Figure 6. COX1/2 are diffusely expressed throughout all granuloma regions

(**a**) COX1/2 are the key enzymes in prostanoid synthesis from AA. (**b**) Average quantitation of COX1/2 fluorescence in granulomas (n = 5). (**c**) Lipid quantitation for 6-keto-PGF1-α, a prostanoid, in the cellular regions of granulomas, mirroring COX1 and COX2 distribution (n = 5). For quantification of fluorescence average intensities in IHC images and for lipid quantification, a student's t-test was performed for single comparisons. For multiple comparisons, mean differences were tested by non-parametric Kruskal-Wallis analysis and adjusted by use of the Bonferoni-Dunn correction. * indicates a *P* value < 0.05 and ** indicate a *P* value < 0.01. (**d**) H&E (upper left) and IHC staining of COX1 (left) and COX2

(right) in green fluorescence, DAPI (blue) and IBA1 (cyan). (**e**) Quantitation of COX1 and COX2 fluorescence as a function of distance from the macrophage border. (**f**) COX1 and COX2 average fluorescence intensity in cellular subtypes within granulomas (n = 7). (**g**) IHC staining of COX1 in cellular and necrotic regions of a rabbit caseous granuloma. TNF-α (red), COX1 (green), nuclei using DAPI (blue), and macrophages using IBA1 (cyan). (**h**) H&E and IHC staining of COX1 in cellular regions of a rabbit solid granuloma. TNF-α (red), COX1 (green), nuclei using DAPI (blue), and macrophages using IBA1 (cyan). All scale bars represent 350 um.